Journal of Power Sources 195 (2010) 4816–4825

Contents lists available at ScienceDirect

Journal of Power Sources

journal homepage: www.elsevier.com/locate/jpowsour

A simple analysis of current collection in tubular solid oxide fuel cells

Anil V. Virkar[a,*], Fred F. Lange[b], Michael A. Homel[c]

[a] Department of Materials Science & Engineering, 122 S. Central Campus Drive, University of Utah, Salt Lake City, UT 84112, United States
[b] Materials Department, University of California, Santa Barbara, CA 93106, United States
[c] Materials and Systems Research, Inc., 5395 West 700 South, Salt Lake City, UT 84104, United States

ARTICLE INFO

Article history:
Received 6 January 2010
Received in revised form 15 February 2010
Accepted 16 February 2010
Available online 20 February 2010

Keywords:
Solid oxide fuel cells
Tubular
Current collection
Portable power
Distributed power

ABSTRACT

A transmission line analysis is presented for the axial current collection in tubular solid oxide fuel cells (SOFC). Closed form analytical solutions are obtained for two modes of current collection: (1) Current collection at one end. (2) Current collection across opposite ends. The analysis shows that cell resistance is lower for current collection at one end compared to that at the opposite ends, with the best case scenario being current collection at both ends. In addition, the analysis shows that for the case of tubular cells, performance may not indefinitely increase with increasing temperature. Experimental data are presented on planar and tubular cells that demonstrate significant differences in temperature dependence. It is projected that under certain conditions, performance of tubular cells may actually decrease with increasing temperature. A design of tubular cells with spines which can substantially lower current collection losses is described.

1. Introduction

Currently both planar and tubular geometries of solid oxide fuel cells (SOFC) are under development by various organizations. The planar geometry is primarily being developed for large scale applications, ranging between ~1 and >10 kW. The modularity of SOFC stacks allows for the construction of hundreds of kW or even MW class systems. Two types of tubular geometries are currently under development. The first is the Siemens–Westinghouse design, in which cathode-supported cells are used with the electrolyte covering part of the cylindrical surface except for a strip for interconnection and anode covering part of the electrolyte surface, which is electrically isolated from the interconnection/cathode [1]. Cell to cell contact is made along the length of the cell using a nickel felt. Thus, current flow through the support electrode (cathode) is ideally circumferential. Systems as large as 200 kW have been demonstrated. The second design uses anode-supported cells of axi-symmetric geometry, in which current collection is at the ends of the cell [2]. In this second design, current flow through electrodes is along the length of the cell. In this geometry, the longer the cell, the greater are the losses associated with current collection. Thus, in this geometry, the design considerations need to address current collection losses. This approach has been primarily used for portable power sources of approximately 20–200 W in size, although larger units of several kW in size have been made and tested. For portable power applications, the cells are typically a millimeter in diameter, and often called micro-tubular SOFC [3,4].

Several authors have addressed the issue of current collection in tubular SOFC. The models vary in degree of complexity and detail. Current collection in tubular SOFC of the Siemens–Westinghouse design has been recently addressed [5,6]. Current collection in micro-tubular SOFC of ~1 mm in diameter and ~1 cm in length has been modeled using simple equivalent circuits [7,8]. Detailed models which take into account momentum, heat, and mass transport and electrochemical coupling have been developed by Cui et al. [9,10] and Zhu and Kee [11]. The analysis by Zhu and Kee [11] also determines species concentrations along the length of the cell.

All of the reported models provide numerical solutions. The ones which take into account detailed transport and multi-dimensional nature of the problem, are not amenable to closed form analytical solutions. Numerical approaches are thus necessary to address such complexities. If the objective is to obtain closed form solutions, however, simplifying assumptions are necessary. Closed form solutions are very useful as they allow the evaluation of the role of various parameters on performance with considerable ease, and also have predictive capability often not possible with numerical solutions.

The objective of this manuscript is to provide an analysis of axial current collection in tubular cells in which cell length is an important consideration. The analysis is based on a transmission line model, which lends itself to simple second order, ordinary differential equations resulting in closed form analytical solutions. The analysis takes into account the electrolyte resistance, cathode and anode polarization resistances, and anode and cathode electronic

* Corresponding author. Tel.: +1 801 581 5396; fax: +1 801 581 4816.
E-mail address: anil.virkar@utah.edu (A.V. Virkar).

0378-7753/$ – see front matter © 2010 Elsevier B.V. All rights reserved.
doi:10.1016/j.jpowsour.2010.02.041

Nomenclature

ρ_e	ionic resistivity of the electrolyte (Ω cm)
t_e	electrolyte thickness (cm)
ρ_a	electronic resistivity of the anode (accounting for any applied current collection layers) (Ω cm)
t_a	anode thickness (including any applied current collection layers) (cm)
ρ_c	electronic resistivity of the cathode (accounting for any applied current collection layers) (Ω cm)
t_c	cathode thickness (including any applied current collection layers) (cm)
λ_a^s	geometric factor of anode spine
λ_c^s	geometric factor of cathode spine
ℓ	cell length (cm)
R_{ct}^a	anode polarization resistance (Ω cm^2)
R_{ct}^c	cathode polarization resistance (Ω cm^2)
$\varphi_a(x)$	anode potential at x (V)
$\varphi_c(x)$	cathode potential at x (V)
E_o	Nernst voltage (V)
E_t	terminal voltage (V)
$I(x)$	current per unit circumference at position x (A cm^{-1})
$I(0)$	net current per unit circumference measured in the external circuit (A cm^{-1})
$I_c(x)$	current per unit circumference through the cathode along the length of the cell (A cm^{-1})
$I_a(x)$	current per unit circumference through the anode along the length of the cell (A cm^{-1})
Q	activation enthalpy (kJ mol^{-1})
$R_i = \rho_e t_e + R_{ct}^a + R_{ct}^c$	net area specific resistance of the cell (Ω cm^2) (local)
$a = \sqrt{((\rho_a/t_a)+(\rho_c/t_c))/\rho_e t_e + R_{ct}^a + R_{ct}^c} = \sqrt{((\rho_a/t_a)+(\rho_c/t_c))/R_i}$	inverse characteristic length (cm^{-1})

resistances. Two types of current collection strategies are evaluated and the corresponding values of cell resistance as a function of cell length are determined. Based on these calculations, strategies for the design of tubular cells are presented. Additionally, the effect of temperature on cell performance is qualitatively addressed. It is shown that differences in the schemes of current collection between planar and tubular cells also translate into fundamental differences in the temperature dependence of stack/bundle performance. Experimental results on the effect of temperature on the performance of a planar (button) cell and a tubular cell are presented.

2. Analysis

In what follows, an analysis is presented for current collection at one end of the cell and at the opposite ends of the cell. Using this analysis, it is shown that the best case scenario consists of current collection at both ends.

2.1. Current leads at one end

The following are simplified calculations of current collection and performance of a tubular SOFC. The calculations are given for unit thickness along the cell circumference. It is assumed that the thicknesses of the various layers are much smaller than the cell diameter, and the cell diameter is much smaller than the cell length.[1] This assumption is consistent with typical cell dimensions, namely, cell thickness ~0.1 cm, cell diameter ~1 cm, and cell length ~10 cm. The calculations are given with the assumption that oxidant and fuel compositions do not vary substantially along the length of the cell, which allows one to assume that the Nernst voltage is the same along the length of the cell. In reality, such an assumption may not be accurate for operation at very high fuel and oxidant utilizations, although it is applicable to the vast majority of practical situations. This assumption also allows for simple analytical solutions and is thus deemed of interest for preliminary design considerations and the selection of design parameters for tubular solid oxide fuel cells (SOFC). These solutions also facilitate the prediction of the temperature dependence of the performance of tubular SOFC, not previously reported in studies based on numerical models.

Fig. 1(a) shows a schematic of a cell of length ℓ with current collection at one end. The lengths of arrows in the electrodes (anode and cathode) qualitatively indicate the magnitude of local current – higher close to the current collection tabs and progressively lower at the opposite end. Within the electrolyte, this is shown qualitatively by the spacing between vertical arrows; smaller distance between arrows closer to the current collection tabs indicating higher local current density. At any position along the length of the tube, x, the magnitudes of the current in the anode and the cathode are the same, but their directions are opposite. Fig. 1(b) is a detailed cross-section of the upper side of the cell showing the directions of currents; this cross-section identifies the various cell parameters. The various resistivities are: ρ_e = electrolyte ionic resistivity (Ω cm); ρ_a = anode electronic resistivity (Ω cm); and ρ_c = cathode electronic resistivity (Ω cm). For the case of graded electrodes, e.g., with applied current collector layers (e.g. copper at anode, silver at cathode), the electronic resistivities refer to appropriate averages including any geometric factors. The various thicknesses are: t_e = electrolyte thickness (cm), t_a = anode thickness (cm), and t_c = cathode thickness. The area specific polarization resistances are: R_{ct}^a = anode polarization resistance (Ω cm^2) and R_{ct}^c = cathode polarization resistance (Ω cm^2). The area specific resistance of a cell element or tri-layer (cathode/electrolyte/anode) is given by $R_i = \rho_e t_e + R_{ct}^a + R_{ct}^c$ in Ω cm^2.

It is assumed that $\rho_e >> \rho_a, \rho_c$, which is typically the case.

An equivalent circuit for an element of the cell between x and $x+dx$ is shown in Fig. 2.

The units of $R_i/dx{\cdot}1$ are Ω. The '1' in the denominator refers to unit length along the circumference. If the cell radius is r, then the resistance of the element will be given by $R_i/dx{\cdot}2\pi r$.

The electrical potential difference between the cathode and the anode at position x is given by

$$\varphi_c(x) - \varphi_a(x) = E_o + R_i \frac{dI(x)}{dx} \tag{1}$$

Eq. (1) is based on simple application of the Ohm's law for the cell element of length dx with internal voltage source E_o. Note also that

$$\varphi_a(x+dx) - \varphi_a(x) = -I(x)\frac{\rho_a}{t_a}dx \tag{2}$$

or

$$\frac{d\varphi_a(x)}{dx} = -I(x)\frac{\rho_a}{t_a} \tag{3}$$

[1] The analysis given here is applicable even if the diameter is not much greater than the thickness, or even if the cell cross-section is not circular (may be elliptical). These geometric factors can be readily included in the analysis without altering the basic approach and the resulting forms of the differential equations.

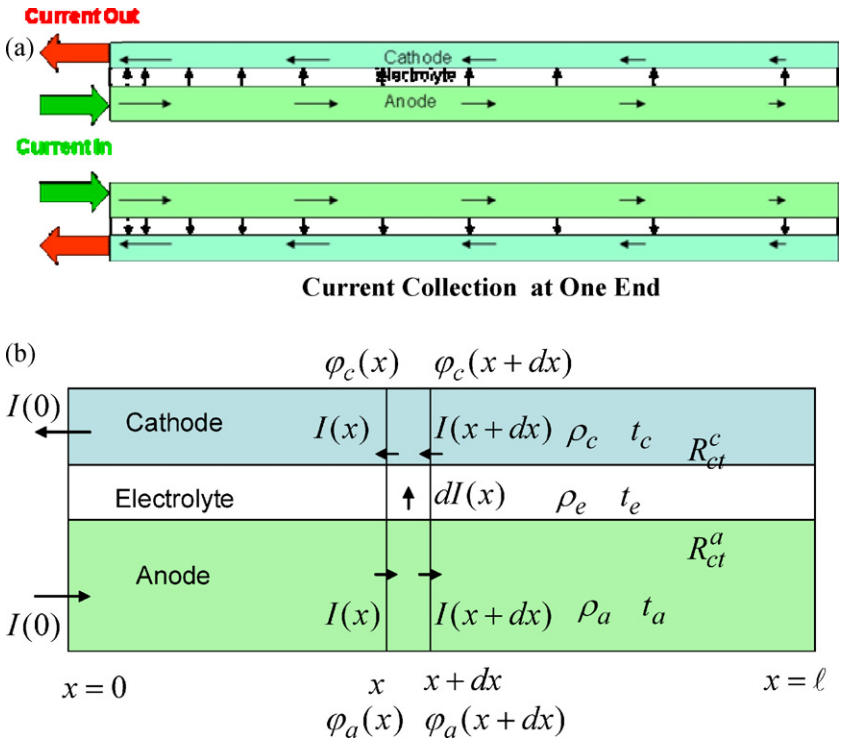

Fig. 1. (a) A schematic of a tubular cell with current leads at one end. (b) A cutout showing the directions of currents and identification of the various parameters.

Similarly,

$$\varphi_c(x) - \varphi_c(x+dx) = -I(x)\frac{\rho_c}{t_c}dx \tag{4}$$

or

$$\frac{d\varphi_c(x)}{dx} = I(x)\frac{\rho_c}{t_c} \tag{5}$$

This gives

$$\frac{d\varphi_c(x)}{dx} - \frac{d\varphi_a(x)}{dx} = \frac{d}{dx}(\varphi_c(x) - \varphi_a(x)) = I(x)\left(\frac{\rho_a}{t_a} + \frac{\rho_c}{t_c}\right) \tag{6}$$

Differentiating Eq. (1) with respect to x, we get

$$\frac{d}{dx}(\varphi_c(x) - \varphi_a(x)) = R_i\frac{d^2I(x)}{dx^2} \tag{7}$$

From Eqs. (6) and (7)

$$R_i\frac{d^2I(x)}{dx^2} = \left(\frac{\rho_a}{t_a} + \frac{\rho_c}{t_c}\right)I(x) \tag{8}$$

which is an ordinary second order differential equation.

One can therefore write

$$a^2 = \frac{(\rho_a/t_a) + (\rho_c/t_c)}{\rho_e t_e + R_{ct}^a + R_{ct}^c} = \frac{(\rho_a/t_a) + (\rho_c/t_c)}{R_i} \tag{9}$$

or

$$a = \sqrt{\frac{(\rho_a/t_a) + (\rho_c/t_c)}{\rho_e t_e + R_{ct}^a + R_{ct}^c}} = \sqrt{\frac{(\rho_a/t_a) + (\rho_c/t_c)}{R_i}} \tag{10}$$

where a has units of cm^{-1}. Thus, the differential equation is

$$\left(\frac{d^2}{dx^2} - a^2\right)I(x) = 0 \tag{11}$$

The general solution to Eq. (10) is

$$I(x) = b_1\ \exp[-ax] + b_2\exp[ax] \tag{12}$$

where b_1 and b_2 are constants.

Note that the voltage difference between the cathode and the anode at position x is given by

$$\varphi_c(x) - \varphi_a(x) = E_o + R_i\frac{dI(x)}{dx} = E_o + R_i\{-b_1 a\exp[-ax] + b_2 a\exp[ax]\} \tag{13}$$

The terminal voltage, E_t, is that corresponding to $x=0$. That is,

$$E_t = \varphi_c(0) - \varphi_a(0) = E_o + R_i a(b_2 - b_1) \tag{14}$$

which gives

$$b_2 = b_1 + \frac{E_t - E_o}{aR_i} \tag{15}$$

We also know that

$$I(\ell) = 0 = b_1\ \exp[-a\ell] + b_2\exp[a\ell] \tag{16}$$

Solving Eqs. (15) and (16), we obtain

$$b_2 = -\frac{E_o - E_t}{aR_i\{1 + \exp[2a\ell]\}} \tag{17}$$

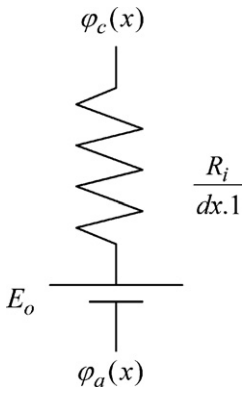

Fig. 2. An equivalent circuit for the cell element between x and $x+dx$.

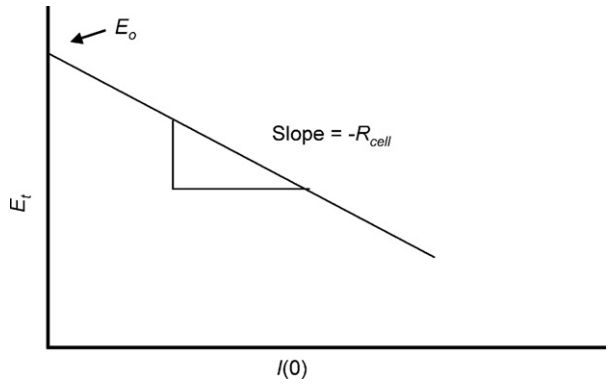

Fig. 3. A schematic of voltage vs. current plot. The magnitude of the slope equals the cell resistance, R_{cell}.

and

$$b_1 = \frac{E_o - E_t}{aR_i}\frac{\exp[2a\ell]}{\{1+\exp[2a\ell]\}} \tag{18}$$

Note that $E_t \le E_o$, thus $b_1 > 0$ and $b_2 < 0$.

The general equation for the potential difference $\varphi_c(x) - \varphi_a(x)$ is given by

$$\varphi_c(x) - \varphi_a(x) = E_o - (E_o - E_t)\left\{\frac{\exp[2a\ell]\exp[-ax] + \exp[ax]}{\exp[2a\ell]+1}\right\} \tag{19}$$

Also note that

$$\frac{dI(x)}{dx} = -\frac{E_o - E_t}{R_i}\frac{\{\exp[2a\ell]\exp[-ax] + \exp[ax]\}}{\{1+\exp[2a\ell]\}} < 0 \tag{20}$$

The terminal current per unit circumference, that is the externally measured current, is given by

$$I(0) = b_1 + b_2 \tag{21}$$

or

$$I(0) = \frac{E_o - E_t}{aR_i}\frac{\{\exp[2a\ell]-1\}}{\{\exp[2a\ell]+1\}} \tag{22}$$

The net power per unit circumference is given by

$$P = E_t I(0) \tag{23}$$

or

$$P = \frac{E_t(E_o - E_t)}{aR_i}\frac{\{\exp[2a\ell]-1\}}{\{\exp[2a\ell]+1\}} \tag{24}$$

The net cell resistance per unit circumference is obtained by plotting the terminal voltage, E_t, vs. the terminal current, $I(0)$, as shown in Fig. 3. Its analytical form is given by

$$R_{cell} = \frac{E_o - E_t}{I(0)} = aR_i\frac{\{\exp[2a\ell]+1\}}{\{\exp[2a\ell]-1\}} \tag{25}$$

We consider a cell of length ℓ. The limits of the cell resistance are as follows.

Limit 1: $2a\ell \to \infty$ (which corresponds to $a \to \infty$ since cell length is finite). This corresponds to a very large sheet resistance, characterized by very high $((\rho_a/t_a) + (\rho_c/t_c))$. This gives $R_{cell} \to aR_i \to \infty$, clearly an undesirable situation.

Limit 2: $2a\ell \to 0$ (which corresponds to $a \to 0$). This corresponds to a negligible sheet resistance, characterized by a very low $((\rho_a/t_a) + (\rho_c/t_c))$. This gives $R_{cell} \to R_i/\ell$. This is the desired situation, but unlikely to be realized in practice.

In the limit the cell length goes to zero, that is as $\ell \to 0$ (for a nonzero a), note that Eq. (25) gives $R_{cell} \to \infty$. This represents cell resistance approaching infinity due to a very small active area. This limit is of no interest as it simply represents negligible active area, and thus is not discussed further. All calculations given here are for a sufficiently large cell length.

Note that we have made calculations for unit circumference. For a tube circumference of $2\pi r$, the net cell resistance is given by

$$R_{cell} = \frac{E_o - E_t}{I(0)} = \frac{aR_i}{2\pi r}\frac{\{\exp[2a\ell]+1\}}{\{\exp[2a\ell]-1\}} \tag{26}$$

For a tube circumference of $2\pi r$, right hand sides of Eqs. (22) and (24) should be multiplied by $2\pi r$ to obtain, respectively net current and net power per cell.

Returning to Eq. (25), the cell resistance attributable to the sheet resistance (current collection) is thus given by

$$R_{sheet} = R_{cell} - \frac{R_i}{\ell} = aR_i\frac{\{\exp[2a\ell]+1\}}{\{\exp[2a\ell]-1\}} - \frac{R_i}{\ell} \tag{27}$$

For a large sheet resistance, the first term may dominate the cell resistance and thus dictate performance. Note that in the limit $\ell \to \infty$, the cell resistance is given by

$$\underset{\ell \to \infty}{\text{Lim}}\, R_{cell} = aR_i \tag{28}$$

and the sheet resistance is given by

$$\underset{\ell \to \infty}{\text{Lim}}\, R_{sheet} = aR_i - \frac{R_i}{\ell} = aR_i \tag{29}$$

That is, in such a case, virtually all of the cell resistance is attributable to the sheet resistance.

2.2. Current leads at opposite ends of the cell (across the length of the cell)

This is the case wherein one of the external leads is connected to the anode at one end, and the other external lead is connected to the cathode at the other end. At the outset, note that as the current leads are connected to opposite ends of the cell, for very long cell lengths, the cell resistance will diverge. Thus, it is understood that current collection cannot be achieved with current leads at opposite ends of cell if the cell is too long. However, it is not unreasonable to expect that for cells not too long, current collection at opposite ends may be an option if it provides practical advantages in design, assembly and operation. The following analysis is given with this purpose in mind. The current collection scheme is shown in Fig. 4(a). A detailed cross-section of the upper side of the cell is given in Fig. 4(b). In this case currents through the anode and the cathode are in the same direction. The total current is fixed, not a function of x, and is a sum of currents through the cathode and the anode. At the left end, the anode current is high but the cathode current is negligible. From left to right, the anode current decreases while the cathode current increases. The lengths of the arrows qualitatively represent the magnitude of the local current.

In this case, both the current in the cathode and the anode are in the same direction. Also, because of Kirchoff's laws, we have

$$I_a(x) + I_c(x) = I \tag{30}$$

where I is the total current.

Thus, note that

$$dI_a(x) = -dI_c(x) \tag{31}$$

Note also that

$$I_a(x) = -\frac{t_a \cdot 1}{\rho_a}\frac{d\varphi_a(x)}{dx} = -\frac{t_a}{\rho_a}\frac{d\varphi_a(x)}{dx} \tag{32}$$

and

$$I_c(x) = -\frac{t_c \cdot 1}{\rho_c}\frac{d\varphi_c(x)}{dx} = -\frac{t_c}{\rho_c}\frac{d\varphi_c(x)}{dx} \tag{33}$$

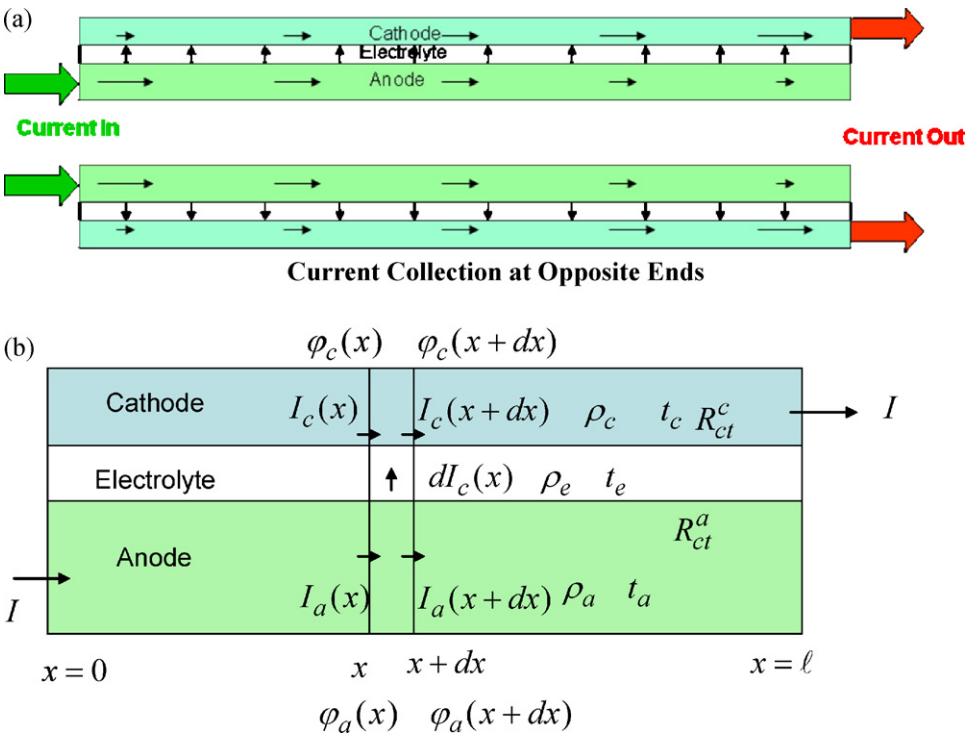

Fig. 4. (a) A schematic of a tubular cell with current leads at opposite ends. (b) A cutout showing the directions of current and identification of the various parameters.

Also, we have

$$\varphi_c(x) - \varphi_a(x) = E_o - R_i \frac{dI_c(x)}{dx} = E_o + R_i \frac{dI_a(x)}{dx} \tag{34}$$

Differentiating Eq. (34)

$$\frac{d\varphi_c(x)}{dx} - \frac{d\varphi_a(x)}{dx} = -R_i \frac{d^2 I_c(x)}{dx^2} = R_i \frac{d^2 I_a(x)}{dx^2} \tag{35}$$

From Eqs. (32), (33), and (35), we can write

$$\frac{d^2 I_c(x)}{dx^2} - a^2 I_c(x) = \left(\frac{d^2}{dx^2} - a^2\right) I_c(x) = -\frac{\rho_a I}{t_a R_i} \tag{36}$$

The general solution to Eq. (36) is given by

$$I_c(x) = b_1' \exp[-ax] + b_2' \exp[ax] + b_3' \tag{37}$$

Substitution of this general solution into Eq. (36) gives

$$b_3' = \frac{\rho_a/t_a}{(\rho_a/t_a)+(\rho_c/t_c)} I \tag{38}$$

Thus,

$$I_c(x) = b_1' \exp[-ax] + b_2' \exp[ax] + \frac{\rho_a/t_a}{(\rho_a/t_a)+(\rho_c/t_c)} I \tag{39}$$

Also, it is seen from Eqs. (30) and (39) that

$$I_a(x) = -b_1' \exp[-ax] - b_2' \exp[ax] + \frac{\rho_c/t_c}{(\rho_a/t_a)+(\rho_c/t_c)} I \tag{40}$$

Again, limiting values of cell resistance can be computed. The limits are as follows.

Limits: When $x = 0$, we have $I_c(x) = 0$.

When $x = \ell$, we have $I_c(x) = I$

Substituting $x = \ell$ into Eqs. (39) and (40), and solving for b_1' and b_2' gives

$$b_1' = -\frac{\{1+(\rho_a/t_a)/((\rho_a/t_a)+(\rho_c/t_c))\{\exp[a\ell]-1\}\}}{\{\exp[a\ell]-\exp[-a\ell]\}} I = b_1'' I \tag{41}$$

where

$$b_1'' = -\frac{\{1+(\rho_a/t_a)/((\rho_a/t_a)+(\rho_c/t_c))\{\exp[a\ell]-1\}\}}{\{\exp[a\ell]-\exp[-a\ell]\}} \tag{42}$$

and

$$b_2' = \frac{\left\{1+(\rho_a/t_a)/((\rho_a/t_a)+(\rho_c/t_c))\{\exp[a\ell]-1\}\right\}}{\{\exp[a\ell]-\exp[-a\ell]\}} I - \frac{\rho_a/t_a}{(\rho_a/t_a)+(\rho_c/t_c)} I = b_2'' I \tag{43}$$

where

$$b_2'' = \frac{\{1+(\rho_a/t_a)/((\rho_a/t_a)+(\rho_c/t_c))\{\exp[a\ell]-1\}\}}{\{\exp[a\ell]-\exp[-a\ell]\}} - \frac{\rho_a/t_a}{(\rho_a/t_a)+(\rho_c/t_c)} \tag{44}$$

Note that b_1' and b_2' are linearly proportional to the net current I, and thus, as-defined, b_1'' and b_2'' are independent of current.

It is easily verified that

$$I_c(0) = b_1' + b_2' + b_3' = 0 \tag{45}$$

Integration of Eqs. (32) and (33) gives

$$\varphi_c(x) = \frac{\rho_c b_1'}{t_c a} \exp[-ax] - \frac{\rho_c b_2'}{t_c a} \exp[ax] - \frac{\rho_c b_3'}{t_c} x + C_1 \tag{46}$$

and

$$\varphi_a(x) = -\frac{\rho_a b_1'}{t_a a} \exp[-ax] + \frac{\rho_a b_2'}{t_a a} \exp[ax] - \frac{\rho_a I}{t_a} x + \frac{\rho_a b_3'}{t_a} x + C_2 \tag{47}$$

We now need to determine the constants C_1 and C_2, which are functions of the other parameters and the net current. Let us set $\varphi_a(0) = 0$, that is the anode at $x = 0$ is connected to ground. This gives

$$C_2 = \frac{\rho_a}{a t_a}(b_1' - b_2') \tag{48}$$

Since b'_1 and b'_2 are linearly proportional to the current I, it is clear that C_2 is also linearly proportional to the current I. From Eq. (34) upon substitution of (46) and (47) we obtain

$$\varphi_c(x) - \varphi_a(x) = E_o + R_i a b'_1 \exp[-ax] - R_i a b'_2 \exp[ax] \tag{49}$$

At open circuit, $I = 0$, thus $b'_1 = 0$, $b'_2 = 0$, and $b'_3 = 0$, and also then

$$\varphi_c(x) - \varphi_a(x) = \varphi_c(x_1) - \varphi_a(x_2) = E_o \tag{50}$$

for any values of x_1 and x_2 along the length of the cell. Note that at open circuit, we also have $\varphi_c(x_1) - \varphi_a(x_2) = C_1^* - C_2^*$, where C_1^* and C_2^* are the constants C_1 and C_2 at open circuit (zero current). But, $C_2^* = 0$, since the current is zero. It is readily seen that $C_1^* = E_o$.

The general expression for $\varphi_c(x) - \varphi_a(x)$ using Eqs. (32) and (33) is given by

$$\varphi_c(x) - \varphi_a(x) = \frac{(\rho_a/t_a) + (\rho_c/t_c)}{a}\{b'_1 \exp[-ax] - b'_2 \exp[ax]\} + C_1 - C_2 \tag{51}$$

Substituting $x = 0$ in Eq. (51) and substituting for C_2 from Eq. (48) gives

$$\varphi_c(0) - \varphi_a(0) = \rho_c \left(\frac{b'_1 - b'_2}{t_c a}\right) + C_1 \tag{52}$$

Also from Eq. (49), we have

$$\varphi_c(0) - \varphi_a(0) = E_o + R_i a (b'_1 - b'_2) \tag{53}$$

From Eqs. (52) and (53), note that

$$C_1 = E_o + \left(R_i a - \frac{\rho_c}{t_c a}\right)(b'_1 - b'_2) \tag{54}$$

Thus, from Eq. (51), the difference, $\varphi_c(x) - \varphi_a(x)$, can be estimated.

Consider the case corresponding to a very low sheet resistance, characterized by $a\ell \to 0$. It can be shown that in this limit

$$b'_1 \to -\frac{I}{2a\ell} \text{ and } b'_2 \to \frac{I}{2a\ell} - \frac{\rho_a/t_a}{(\rho_a/t_a) + (\rho_c/t_c)} I \to \frac{I}{2a\ell}$$

and, the corresponding potential difference is given by

$$\varphi_c(x) - \varphi_a(x) = \varphi_c(x_1) - \varphi_a(x_2) = E_o - I\frac{R_i}{\ell} \tag{55}$$

That is, for zero sheet resistance, the total cell resistance is given by $R_i/\ell \cdot 1$ in ohms, which not surprisingly, is identical to the case where the external leads are connected to one end of the cell. This is because if both the anode and the cathode are highly conductive, they are equi-potential regions. For this reason, under such conditions, $\varphi_c(x_1) - \varphi_a(x_2)$ is independent of position along the cathode and anode surfaces, and is given by Eq. (55). This is the desired situation, but unlikely to be realized in practice.

Now our objective is to obtain

$$\varphi_c(\ell) - \varphi_a(0) = \phi_c(\ell) = E_t \tag{56}$$

where E_t is the terminal voltage (across the length of the cell). Then, the net cell resistance per unit circumference is given by

$$R_{cell} = \frac{E_o - E_t}{I} \tag{57}$$

The general equation for $\varphi_c(x)$ upon substitution for C_1 from Eq. (54) into (46) is given by

$$\varphi_c(x) = E_o + \frac{\rho_c b'_1}{t_c a} \exp[-ax] - \frac{\rho_c b'_2}{t_c a} \exp[ax] - \frac{\rho_c b'_3}{t_c} x + \left(aR_i - \frac{\rho_c}{a t_c}\right)(b'_1 - b'_2) \tag{58}$$

Thus, the terminal voltage is given by

$$E_t = \varphi_c(\ell) = E_o + \frac{\rho_c b'_1}{t_c a} \exp[-a\ell] - \frac{\rho_c b'_2}{t_c a} \exp[a\ell] - \frac{\rho_c b'_3}{t_c} x + \left(aR_i - \frac{\rho_c}{a t_c}\right)(b'_1 - b'_2) \tag{59}$$

Therefore, the net cell resistance per unit circumference from Eqs. (38), (42), (44), (57) and (59) is given by

$$R_{cell} = \left\{ -\frac{\rho_c b''_1}{t_c a} \exp[-a\ell] + \frac{\rho_c b''_2}{t_c a} \exp[a\ell] + \frac{\rho_a \rho_c / t_a t_c}{(\rho_a/t_a) + (\rho_c/t_c)} \ell - (b''_1 - b''_2)\left(aR_i - \frac{\rho_c}{a t_c}\right) \right\} \tag{60}$$

The net current per unit circumference is given by

$$I = \frac{E_o - E_t}{R_{cell}} \tag{61}$$

and the net power per unit circumference is given by

$$P = E_t I = \frac{E_t(E_o - E_t)}{R_{cell}} \tag{62}$$

Eqs. (60), (61) and (62) are for unit circumference. For a circumference of $2\pi r$, the requisite values are obtained by dividing the right hand side of Eq. (60) by $2\pi r$ to obtain the net cell resistance, and multiplying the right hand sides of Eqs. (61) and (62) by $2\pi r$ to obtain, respectively the net current and the net power.

Returning to Eq. (60), note that the cell resistance attributable to the sheet resistance is given by

$$R_{sheet} = R_{cell} - \frac{R_i}{\ell} \tag{63}$$

where R_{cell} is given by Eq. (60). An examination of Eq. (60) shows that as the cell length goes to infinity, the R_{cell} also goes to infinity. That is,

$$R_{cell} \to \infty \quad \text{Lim}\ \ell \to \infty \tag{64}$$

and

$$R_{sheet} \to \infty \quad \text{Lim}\ \ell \to \infty \tag{65}$$

This of course is to be expected as current collection is across opposite ends of the cell. Thus, if cell length goes to infinity, the cell resistance also goes to infinity. Obviously, cell length cannot be too large if this mode of current collection is selected for any possible practical and design advantages.

2.3. Comparison between current leads at one end vs. current leads at opposite ends

The relevant equations for the cell resistance are Eqs. (25) and (60). It is clear that the two values of R_{cell}, not surprisingly, are different. We have seen, however, that in the limit $a\ell \to 0$ (very low sheet resistance), both solutions approach an identical limit. As a further verification of the two equations, we will consider the limits for two cases; a highly conductive anode and a highly conductive cathode.

2.4. Anode is highly conductive, that is $\rho_a/t_a \to 0$, but not the cathode

In such a case, the anode is an equi-potential region. Thus, in this case, both solutions should approach an identical limit. It can be readily shown that this in fact is the case. That is, both Eqs. (25)

Table 1
Calculated cell resistance and sheet resistance (given in parentheses) for current collection at one end, at opposite ends, their ratio, and cell resistance for current collection at both ends.

ρ_a (Ω cm)	ρ_c (Ω cm)	R_{cell} (Ω cm) current collection at one end (sheet resistance)	R_{cell} (Ω cm) current collection at opposite ends (sheet resistance)	Ratio	R_{cell} (Ω cm) current collection at both ends (sheet resistance)
10^{-3}	10^{-2}	0.1658 (0.1408)	0.2298 (0.2048)	1.386	0.08313 (0.05813)
10^{-3}	10^{-3}	0.0712 (0.0462)	0.0898 (0.0648)	1.2612	0.0398 (0.0148)
10^{-4}	10^{-4}	0.0313 (0.0063)	0.0317 (0.0067)	1.0128	0.02664 (0.00164)

and (60) exhibit the following limit when ρ_a/t_a is set to zero in Eqs. (25) and (60), namely

$$R_{cell} = \sqrt{\frac{\rho_c R_i}{t_c}}\,\frac{\{\exp[2a\ell]+1\}}{\{\exp[2a\ell]-1\}} \tag{66}$$

Note that in this case

$$a = \sqrt{\frac{\rho_c}{t_c R_i}} = \sqrt{\frac{\rho_c}{t_c(\rho_e t_e + R^a_{ct} + R^c_{ct})}} \tag{67}$$

2.5. Cathode is highly conductive, that is $\rho_c/t_c \to 0$, but not the anode

In such a case, the cathode is an equi-potential region. Thus, in this case also, both solutions should approach an identical limit. It can be readily shown that both Eqs. (25) and (60) exhibit the following limit when ρ_c/t_c is set to zero in Eqs. (25) and (60), namely

$$R_{cell} = \sqrt{\frac{\rho_a R_i}{t_a}}\,\frac{\{\exp[2a\ell]+1\}}{\{\exp[2a\ell]-1\}} \tag{68}$$

Note that in this case

$$a = \sqrt{\frac{\rho_a}{t_a R_i}} = \sqrt{\frac{\rho_a}{t_a(\rho_e t_e + R^a_{ct} + R^c_{ct})}} \tag{69}$$

2.6. Current leads at both ends

An extension of the two modes of current collection is the third case, where the current is collected at both ends. The corresponding solution is simply the resistance corresponding to half the cell length with current collection at one end divided by two. That is, for this case, the net cell resistance is given by

$$R_{cell} = \frac{E_o - E_t}{I(0)} = \frac{aR_i}{2}\,\frac{\{\exp[a\ell]+1\}}{\{\exp[a\ell]-1\}} \tag{70}$$

The preceding equation represents the resistance of the cell when anode current collection tabs are connected to each other and cathode current collection tabs are connected to each other. As the cell length goes to infinity, the limiting values of the cell resistance and sheet resistance are

$$\underset{\ell \to \infty}{\text{Lim}}\, R_{cell} = \frac{aR_i}{2} \tag{71}$$

and

$$\underset{\ell \to \infty}{\text{Lim}}\, R_{sheet} = \frac{aR_i}{2} - \frac{R_i}{\ell} = \frac{aR_i}{2} \tag{72}$$

Note that as the cell length goes to infinity, the cell resistance for current collection at both ends (Eq. (71)) is exactly half that for the case where the current collection is only at one end (Eq. (28)).

2.7. Numerical calculations

In what follows, numerical calculations are presented with the objective being to compare the two different cases, and determine which arrangement gives the lowest cell resistance and thus the highest performance. That is, the objective is to determine if the external leads should be connected to the cathode and the anode at the same end or the opposite ends.

We will assume $R_i = 0.25\,\Omega\,\text{cm}^2$, $t_a = 0.1$ cm, $t_c = 0.1$ cm, and $\ell = 10$ cm. Thus, the cell resistance per unit circumference without including the sheet resistance is given by $R_i/\ell = 0.025\,\Omega$ cm. Table 1 gives the calculated R_{cell} (for unit circumference) for the three cases – current leads at one end, current leads at opposite ends, and current leads at both ends.

Table 1 shows that the cell resistance is higher if the current leads are at opposite ends (external terminals connected to the cathode and the anode at the opposite ends of the cell) rather than at one end. The higher the sheet resistance, the greater is this difference. Thus, it is preferable to connect the current leads at one end, especially if the sheet resistance is high. The best case scenario is when current is collected at both ends. The corresponding resistance is also given in this table.[2] If the electrical conductances of both the cathode and the anode are very high so that both can be considered as equi-potential surfaces, all three modes of current collection give the same cell resistance. In practice, this is generally not possible for cell lengths of interest (several cm or a few tens of cm). Thus, a suitable choice should be made. Again, the best choice is current collection at both ends.

The table also gives contribution of the sheet resistance to the total cell resistance. Note that for anode and cathode resistivities of 10^{-3} and $10^{-2}\,\Omega$ cm (and higher), respectively, for a 10 cm long cell, the sheet resistance dominates the net resistance. The implications of these results concerning the temperature dependence of cell performance are discussed in what follows.

2.8. Temperature dependence of cell performance

In a planar fuel cell stack (or a repeat unit comprising a cell and an interconnect), usually the main contribution to the total resistance is due to the cell and the contact resistances. The sheet resistance is typically small. Thus, for a planar cell/stack, the main contribution to the area specific resistance is from R_i and possible contact resistances. The terms in R_i are; ρ_e = the ionic resistivity of the electrolyte, R^a_{ct} = the anode activation polarization resistance, and R^c_{ct} = the cathode activation polarization resistance. All these three contributions are thermally activated; they decrease with increasing temperature. Thus, in planar cells/stacks, the performance generally increases with increasing temperature. Fig. 5 shows plots of voltage and power density vs. current density for a

[2] This result is in agreement with prior published numerical results [7–10]. The present closed form analytical solutions permit the evaluation of the role of various parameters in a straightforward manner, which is difficult using numerical approaches.

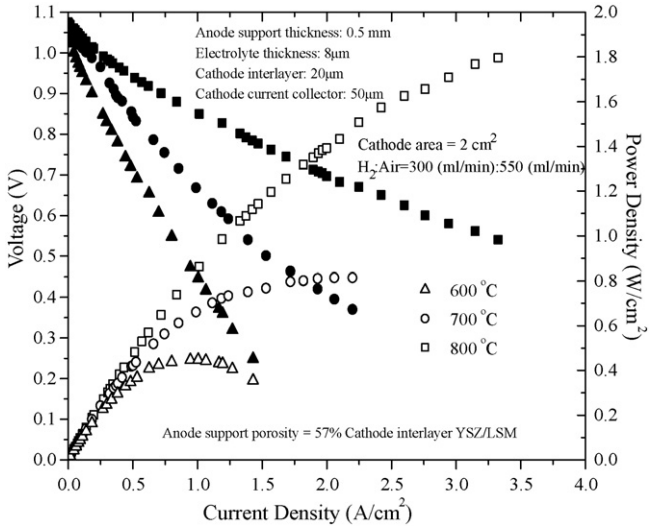

Fig. 5. Performance curves (LSM + YSZ/YSZ/Ni + YSZ) on a button (planar) solid oxide fuel cell. Note the increase in power density between 600 and 800 °C with increasing temperature. In this case, current collection losses are small.

planar button cell over the temperature range from 600 and 800 °C. Note the rapid rise in power density with increasing temperature in Fig. 5.

In tubular cells, as discussed herein, the sheet resistance due to the current path along the length of the cell can be significant. Table 1 shows for example that for typical values of electronic resistivities of cathode and anode, ρ_a and ρ_c, a significant contribution to the net cell resistance in a 10 cm long cell is due to the sheet resistance. The anode typically contains Ni metal. Its resistivity ρ_a increases with increasing temperature. Temperature coefficients of resistivities of most metals are well known and can be found in standard handbooks. In most cases, the cathode is a perovskite containing transition metal ions. Depending upon the dopant concentration and temperature, these materials can also exhibit metallic behavior at high temperatures – that is, in many cases, ρ_c also increases with increasing temperature. Additionally, often a silver screen is used as a current collector at the cathode, whose resistance increases with increasing temperature. Thus, as the temperature increases, the R_i decreases but ρ_a and ρ_c increase.

At low temperatures, the R_i will likely be large and will dictate performance. The net effect is that depending upon the relative values of the various parameters, the net cell resistance, R_{cell}, will initially decrease with increasing temperature thus increasing performance with increasing temperature. This for example is the case with studies on micro-tubular SOFC conducted at low temperatures by Suzuki et al. [8]. However, at sufficiently high temperatures, and depending upon the cell length, the R_i may become a small part of the total cell resistance. Under such conditions, the net R_{cell} can actually increase with increasing temperature. As a result, the cell performance will initially increase with increasing temperature, but it may later actually decrease with increasing temperature.

A qualitative assessment of the temperature dependence of the cell resistance, R_{cell}, can be readily made to determine the minimum cell resistance achievable as a function of temperature. This is discussed in what follows. Consider for example current collection at both ends, given by Eq. (70) reproduced below:

$$R_{cell} = \frac{E_o - E_t}{I(0)} = \frac{aR_i}{2}\frac{\{\exp[a\ell]+1\}}{\{\exp[a\ell]-1\}} = \frac{\sqrt{R_i((\rho_a/t_a)+(\rho_c/t_c))}}{2}\frac{\{\exp[a\ell]+1\}}{\{\exp[a\ell]-1\}} \quad (73)$$

The anode and cathode (including current collection layers which are metallic) are expected to exhibit temperature dependence of the form

$$\left(\frac{\rho_a}{t_a}+\frac{\rho_c}{t_c}\right) \approx A + BT \quad (74)$$

where A and B are positive constants. The area specific resistance of the tri-layer (cathode–electrolyte–anode), R_i, contains all terms that obey Arrhenius-type relations. In most cases over a typical temperature range of interest, the R_i may be given by an equation of the form

$$R_i \approx R_i^o \exp\left[\frac{Q}{RT}\right] \quad (75)$$

where R_i^o is a constant and Q is the activation enthalpy. An examination of Eqs. (10) and (73) show that as the temperature increases, $a\ell$ increases, and the factor $\{\exp[a\ell]+1\}/\{\exp[a\ell]-1\}$ decreases. The lowest possible value $\{\exp[a\ell]+1\}/\{\exp[a\ell]-1\}$ can have is unity. The factor $\sqrt{(R_i((\rho_a/t_a)+(\rho_c/t_c)))/2}$ is of the form $((A+BT)\exp[Q/RT])^{1/2}$. Note that as the temperature approaches zero (mathematical limit only), the factor $((A+BT)\exp[Q/RT])^{1/2}$ goes to infinity. Note also that as the temperature goes to infinity, the factor $((A+BT)\exp[Q/RT])^{1/2}$ goes to infinity. Clearly, the factor $((A+BT)\exp[Q/RT])^{1/2}$ goes through a minimum at some temperature. The preceding discussion shows that the R_{cell} itself goes through a minimum at some temperature. If the temperature dependencies of ρ_a, ρ_c, R_i are known and all geometric parameters are known, it is a straightforward matter to determine the temperature at which the lowest possible cell resistance (including current collection) occurs by setting the derivative of R_{cell} with temperature to zero; that is,

$$\frac{dR_{cell}}{dT} = 0 \quad (76)$$

This allows for the determination of the temperature at which a tubular cell should be operated to obtain the maximum performance. The value of simple closed form solutions, such as the ones presented here, lies in their ability to describe the functional dependence on various operating parameters (such as temperature dependence demonstrated here) which is generally not possible with numerical solutions. Once preliminary design parameters (e.g. electrode thicknesses and cell length for a given set of fundamental parameters, namely ρ_e, ρ_a, ρ_c, R_{ct}^a, and R_{ct}^c) have been identified using the analytical model described here, the next step will be to conduct a detailed numerical analysis for fine tuning.

Fig. 6 shows the results of performance tests on a tubular cell over a temperature range between 650 and 850 °C. It is to be noted that the observed increase in performance with increasing temperature is modest compared to that observed for the planar cell (Fig. 5). Also, it is observed that the performance increase between 800 and 850 °C is much lower than between 750 and 800 °C, which is lower than between 700 and 750 °C. Note also the performance of the tubular cell is lower than that of the planar cell even though the cell materials and microstructures of the two cells are essentially the same. This is consistent with the analysis and discussion presented here. This is because with increasing temperature, the sheet resistance increases, and becomes the dominant contribution. It is expected that at even higher temperatures, the performance of tubular cells may actually decrease with increasing temperature. Thus, when using tubular cells, an indefinite increase in cell performance with increasing temperature is not expected, unlike in planar cells.[3] From an experimental standpoint, whenever an

[3] Even in planar cells, sheet resistance can be significant if the distance between current collection ribs is too large as discussed previously [12].

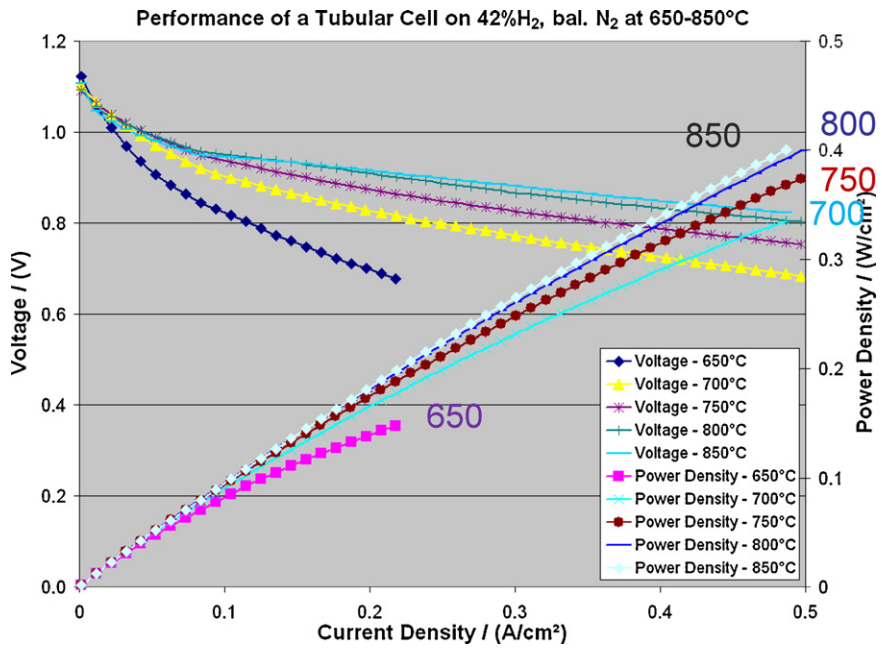

Fig. 6. Performance tests on a tubular solid oxide cell over a temperature range between 650 and 850 °C. Note that the performance increase with increasing temperature between 750 and 850 °C is modest. This is due to the performance being limited by current collection losses. Note also the lower power density compared to the planar (button) cell.

observation is made that cell performance does not appear to significantly increase with increasing temperature, it is an indication that current collection losses are limiting the overall performance.

2.9. Current collection spines

The present analysis and experimental observations have demonstrated that significant losses occur in current collection in tubular solid oxide fuel cells. This conclusion is in accord with prior reported work [7–11]. A possible approach to minimizing voltage losses is to introduce current collection 'spines' on both the cathode and the anode [13]. A schematic of one such design is shown in Fig. 7. Although not shown in Fig. 7, the spines extend beyond the circular cells so that the external connections are made outside of the hot zone. The objective is to design the spines such that the term $((\rho_a/t_a)+(\rho_c/t_c))$ is made as small as possible. The calculations can be readily extended to the case with multiple layers. The spines can be made respectively of the same materials as the cathode and anode but of higher density (lower porosity) to lower their electronic resistivities while at the same time minimizing stresses related to thermal expansion mismatch. If ρ_a^s and ρ_c^s are respectively the electronic resistivities of the anode and cathode spines, t_a^s and t_c^s are respectively anode and cathode spine thicknesses, and if λ_a^s and λ_c^s are respectively dimensionless parameters describing the geometries of the anode and cathode spines which account for differing cross-sectional geometries, then the term $((\rho_a/t_a)+(\rho_c/t_c))$ may be replaced by $(\overline{(\rho_a/t_a)}+\overline{(\rho_c/t_c)})$, where

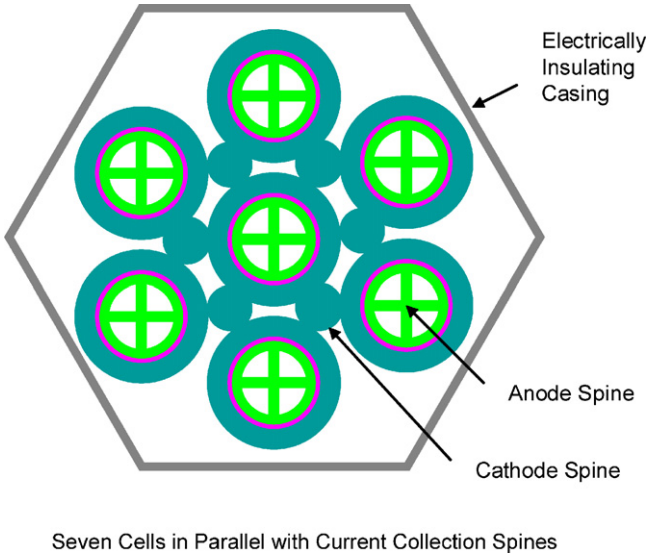

Fig. 7. Seven cells connected in parallel with cathode and anode current collection spines. The spines are designed (materials and thicknesses) to ensure minimal current collection losses and minimal stresses. The hexagonal housing is an electrical insulator. Connections are made at the ends.

$$\overline{\left(\frac{\rho_a}{t_a}\right)} = \frac{1}{(t_a/\rho_a)+\lambda_a^s(t_a^s/\rho_a^s)} \tag{77}$$

and

$$\overline{\left(\frac{\rho_c}{t_c}\right)} = \frac{1}{(t_c/\rho_c)+\lambda_c^s(t_c^s/\rho_c^s)} \tag{78}$$

Our objective is to design the spines (materials and geometries), such that $(\overline{(\rho_a/t_a)}+\overline{(\rho_c/t_c)})$ is as small as possible. We will thus define the parameter a by the following equation, namely

$$a = \sqrt{\frac{\overline{(\rho_a/t_a)}+\overline{(\rho_c/t_c)}}{\rho_e t_e + R_{ct}^a + R_{ct}^c}} = \sqrt{\frac{\overline{(\rho_a/t_a)}+\overline{(\rho_c/t_c)}}{R_i}} \tag{79}$$

Our objective then is to make a as small as possible (for a given R_i), while still ensuring as low an R_i as possible. In typical anode-supported cells made using standard materials (YSZ, LSM, and Ni), it is possible to achieve $R_i \sim 0.25\ \Omega\,\mathrm{cm}^2$, and as low as $\sim 0.15\ \Omega\,\mathrm{cm}^2$ at 800 °C. Even smaller values are possible. The smaller the value of R_i, the more important it is to design the spines for the best possible current collection.

3. Summary

A transmission line model is presented which leads to closed form solutions for the cell resistance of tubular solid oxide fuel cells with axial current collection. The model takes into account various specific resistances of the electrolyte, the electrodes, the polarization resistances, electrode (current collector) thicknesses, and the cell length. Two modes of current collection were analyzed; one where the current collection is at one end, and the other where the current collection is at opposite ends. Simple second order ordinary differential equations were obtained and solved to determine the net cell resistance. They include contributions from the fundamental cell parameters, namely, the electrolyte specific resistance, polarization specific resistances and resistance associated with the transmission of current along the length of the cell to current collection tabs. The cell resistance is lower for current collection at one end. The best case scenario consists of current collection at both ends, for which the cell resistance is the lowest. This mode of current collection also has the advantage of a built-in redundancy – even if a cell is damaged in the middle, current collection continues at some level thus increasing the overall efficiency.

In tubular cells, the sheet resistance associated with current collection can dominate cell resistance and thus cell performance. The sheet resistance is primarily associated with current collection, which typically includes metallic materials whose electrical resistance increases with increasing temperature. If the sheet resistance is large, the cell performance may not continue to increase with increasing temperature unlike planar cells, but may in fact decrease with increasing temperature. This an important consideration in the design of tubular SOFC typically not encountered in the design of planar stacks. An effective way to minimize current collection losses in tubular SOFC is the introduction of spines. A design incorporating spines is proposed.

The results of analysis presented can be readily used to design tubular SOFC provided fundamental parameters have been measured on given cell/materials, e.g., ρ_e, ρ_a, ρ_c, R^a_{ct}, and R^c_{ct}, and preferably over a range of temperatures. Such measurements can be made on small button cells and specially prepared samples for characterization. Then using Eq. (25) for current collection at one end or Eq. (70) for current collection at both ends, the cell resistance can be estimated for given values of various thicknesses and cell length. This information can be used for design purposes. If the temperature dependence of the various parameters is known, the operating temperature at which the best performance can be realized can also be determined by the procedure described here.

Acknowledgement

This work was supported in part by the US Department of Energy under Grant Number DE-FG02-06ER46086.

References

[1] S.C. Singhal, Solid State Ionics 135 (2000) 305–313.
[2] N.M. Sammes, Y. Du, R. Bove, J. Power Sources 145 (2005) 428–434.
[3] T. Suzuki, Y. Funahashi, T. Yamaguchi, Y. Fujishiro, M. Awano, J. Power Sources 171 (2007) 92–95.
[4] P. Sarkar, L. Yamarte, H. Rho, L. Johanson, Int. J. Appl. Ceram. Technol. 4 (2) (2007) 103–108.
[5] G. DiGiuseppe, R. Draper, J. Fuel Cell Sci. Technol. 5 (2008) 021013-1–021013-9.
[6] J.-M. Klein, Y. Bultel, M. Pons, P. Ozil, J. Appl. Electrochem. 38 (2008) 497–505.
[7] T. Suzuki, T. Yamaguchi, Y. Fujishiro, M. Awano, J. Power Sources 163 (2007) 737–742.
[8] T. Suzuki, Y. Funahashi, T. Yamaguchi, Y. Fujishiro, M. Awano, J. Power Sources 175 (2008) 68–74.
[9] D. Cui, L. Liu, Y. Dong, M. Cheng, J. Power Sources 174 (2007) 246–254.
[10] D. Cui, M. Cheng, AIChE J. 55 (3) (2009) 771–782.
[11] H. Zhu, R.J. Kee, J. Power Sources 169 (2007) 315–326.
[12] C.W. Tanner, A.V. Virkar, J. Power Sources 113 (2003) 44–56.
[13] F.F. Lange, A.V. Virkar, US Patent, Application 'Advanced Solid Oxide Fuel Cell Stack for Power Generation', July 2005.